Check for updates

Leaching of iron from copper tailings by sulfuric acid: behavior, kinetics and mechanism†

Lei Tao,[a] Langlang Wang,[a] Kanghuai Yang,[a] Xueqian Wang, [ID] *[a] Lu Chen*[b] and Ping Ning[a]

Copper tailing is a widespread and intractable solid waste in copper production. Traditional leaching and recovery technology for copper tailing focuses on copper but neglects the leaching of iron. With the increase in applications and demands of iron-containing materials for environment, understanding the leaching behaviors of iron can promote the utilization of copper tailings. In this study, the kinetics and mechanism of the leaching of iron from copper tailings using sulfuric acid were studied. Under optimal conditions (40 °C, sulfuric acid concentration of 0.53 mol L^{-1}, stirring speed of 400 rpm, solid/liquid ratio of 1 : 10 and leaching time of 120 min), 66.45% of Fe, along with 65.32% of Zn and 59.95% of Cu, were leached from the tailings. The leaching of iron was confirmed to be controlled by solid-film diffusion. The reaction orders for sulfuric acid concentration, solid/liquid ratio, and stirring speed were found to be 0.85, −0.70, and 0.40, respectively. Results from XRF, XRD, and SEM indicated that oxides (including CaO, CuO, and ZnO) were leached first, after which Fe_2SiO_4 was preferentially reacted compared to Fe_3O_4. The accumulation of $CaSO_4$ and SiO_2 inhibited the further leaching of iron.

1. Introduction

Copper tailing is the residual ore left after copper extraction during a floatation process, which is more difficult to recycle as compared to the copper slag. Its main components are fayalite (Fe_2SiO_4) and magnetic iron oxide (Fe_3O_4), accounting for more than 55% of the copper tailings.[1] In 2015, it is estimated that 68.7 million tons of copper tailings were produced worldwide.[2] Copper tailing is often discarded into stock dumps or sold for use in cement and roadbed production.[3,4] These methods not only waste limited mineral resources but also potentially damage the ecological environment.[5,6] Recently, several approaches for more comprehensive utilization of copper slag have focused on pyrometallurgy. Green reductants, such as walnut shell char,[7] and waste cooking oil,[8] were employed to recycle iron from the waste copper slag. Fuentes *et al.*[9] have also used reduced copper slag as a catalyst for carbon oxide hydrogenation. However, traditional pyrometallurgy is expensive and requires a large amount of energy consumption.

Hydrometallurgy is another way to recycle metals with more convenience and less energy consumption.[10] If the goal is the separation of valuable metals, the leaching of iron and silicon ions is undesirable. In these cases, bioleaching[11,12] and high-pressure leaching[13,14] can be used to recycle copper. On the other hand, metal ions contribute to the liquid catalytic oxidation of SO_2,[15,16] and elements such as iron and silicon are important components for water treatment[17–19] and soil remediation.[20] Thus, it is important to explore the leaching behavior of metals in copper tailings to improve the application possibility of copper tailings. Rogowski *et al.*[21] used various acids for the dissolution of metals from copper flotation tailings. However, to the best of our knowledge, the acid leaching behavior with respect to iron has rarely been reported.

Herein, a theoretical analysis of the leaching of iron from copper tailings was performed. Then, the effects of key factors on iron leaching were investigated, including the reaction temperature, sulfuric acid concentration, ratio of solid to liquid (S/L ratio), and stirring speed. The kinetics of leaching was also analyzed based on a shrinking model. The behavior of Ca, Zn, Cu, and Si in the leaching process was also studied. Characterizations including X-ray fluorescence (XRF), X-ray diffraction (XRD), X-ray photoelectron spectroscopy (XPS), scanning electron microscopy (SEM), Fourier transform infrared spectroscopy (FTIR), as well as the measurements of particle size distribution (PSD), and magnetic properties were investigated to reveal the leaching behavior of copper tailings.

[a]*Faculty of Environmental Science and Engineering, Kunming University of Science and Technology, Kunming 650500, PR China. E-mail: wxq3000@aliyun.com; Tel: +86 13888183303*

[b]*Faculty of Business Management, Yunnan Communications Vocational and Technical College, Kunming 650500, PR China. E-mail: 175394073@qq.com*

2. Experimental

2.1. Materials

The copper tailings used in this study were obtained from the Yunnan Tin Group (Holding) Company Limited, China. The major element components present in the copper tailings are shown in Table 1. Other chemicals, including H_2SO_4 (98%, Xilong Chemical Group Co. Ltd.), were of analytical grade.

2.2. Instruments and procedure

Fig. 1 shows the set-up used to study the leaching process of copper tailings. The experiments were performed according to the following procedure. First, 200 mL of the leaching agent was prepared using H_2SO_4 and deionized water, and poured into a three-necked round-bottom flask. The leaching agent was heated to the desired temperature. Then, the copper tailings were added into the flask at the set speed. At the desired time interval, 4 mL of the solution was removed and filtered. The iron ion concentration in the filtrate was measured *via* titration.[15] The Ca^{2+}, Zn^{2+}, Cu^{2+} and Si^{4+} ion concentration in the filtrate was measured using ICP-OES (Agilent 730). Each sulfuric acid leaching experiments of copper tailings was repeated three times, and the average value of these three values was used to reported to avoid any errors.

The metal ion leaching rate for Fe^{2+}, Ca^{2+}, Zn^{2+}, Cu^{2+} and Si^{4+} was calculated using eqn (1).

$$X = \frac{C_a V}{w_s m} \times 100\% \tag{1}$$

where X is the leaching rate of the target metal, %; C_a is the ion concentration in the leachate, mg L^{-1}; V is the volume of leachate, L; w_s is the elemental content of the target metal in the copper tailings, wt%; and m is the mass of copper tailing, g.

2.3. Kinetic analysis

In a heterogeneous solid/liquid leaching reaction system, the soluble reactants diffuse across the interface and/or through the solid layer first.[22,23] The leaching is generally controlled by either diffusion through the product layer, chemical reaction at the surface of the solid particles or a mixture of diffusion and chemical reaction.

If the leaching is controlled by diffusion through the product layer, it will follow the rate equation,[23] expressed in eqn (2).

$$1 - (2/3)X - (1-X)^{2/3} = k_d t \tag{2}$$

If the leaching is controlled by the chemical reaction at the surface of the solid particles, it will follow the rate equation,[23] expressed in eqn (3).

$$1 - (1-X)^{1/3} = k_r t \tag{3}$$

where X is the fraction reacted for iron; k_d and k_r are the rate constants for diffusion through the product layer and chemical reaction at the surface of the solid particles (min^{-1}), respectively, and t is the leaching time (min).

The apparent activation energy can be obtained using eqn (4).

$$\ln k = \ln A - \frac{E_a}{RT} \tag{4}$$

where A is the frequency factor, E_a is the apparent activation energy, R is the ideal gas constant (8.314 J mol^{-1} K^{-1}), and T is the leaching temperature (K).

2.4. Characterization of the samples

The elemental composition of the copper tailings before and after the leaching reaction was detected using an XRF spectrometer (PANalytical Axios, Holland). The crystalline phases of the tailings were identified *via* XRD (D8 Advance, Germany) with Cu Kα radiation ($\alpha = 0.154056$ nm). XPS (Thermo Fisher, USA) was used to identify the states of the main elements in the samples. Surface morphology and composition were identified *via* SEM (GeminiSEM 300, Germany) with EDS (Oxford X-MAX, Germany). The functional groups and particle size distribution in the samples were recorded using an FTIR (Bruker Vertex 70, Germany) and a laser diffraction particle size analyzer (Mastersizer 3000, USA). Magnetic properties were determined using a vibrating sample magnetometer (PPMS-9, USA).

Table 1 The XRF analysis of copper tailings before and after leaching

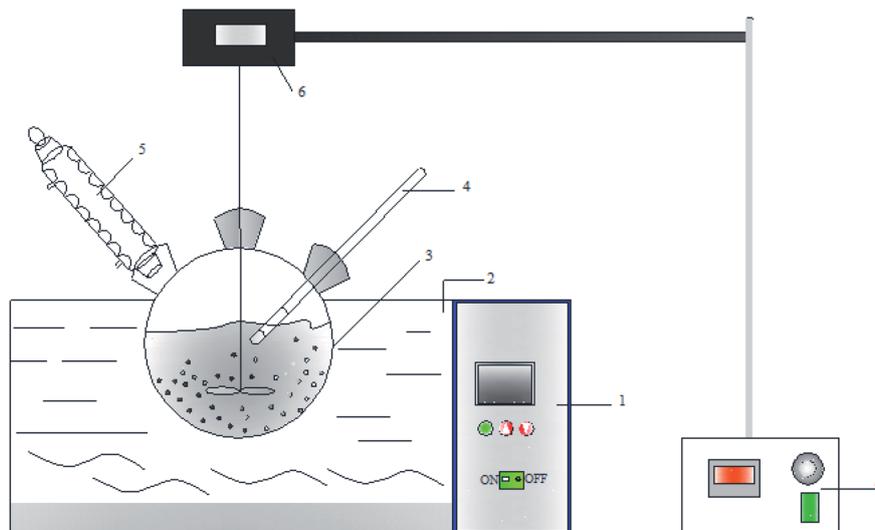| Component	Raw copper tailings (wt%)	Copper tailings after 1 h leaching (wt%)	Copper tailings after 2 h leaching (wt%)
Fe	36.76	28.49	28.44
Si	14.25	17.16	17.11
Ca	3.06	4.65	5.00
Al	2.45	3.62	3.76
Zn	2.06	1.65	1.69
Mg	1.03	0.32	0.29
Na	0.88	0.78	0.77
K	0.44	0.57	0.59
Cu	0.26	0.25	0.24
S	0.17	0.69	0.65
As	0.17	0.21	0.22
Mn	0.11	0.06	0.05

Fig. 1 Diagram of the setup used to study the leaching process: 1 – water bath thermostat; 2 – water bath; 3 – three necked round-bottom flask; 4 – thermometer; 5 – condenser; 6 – mechanical agitator; 7 – stirring speed controller.
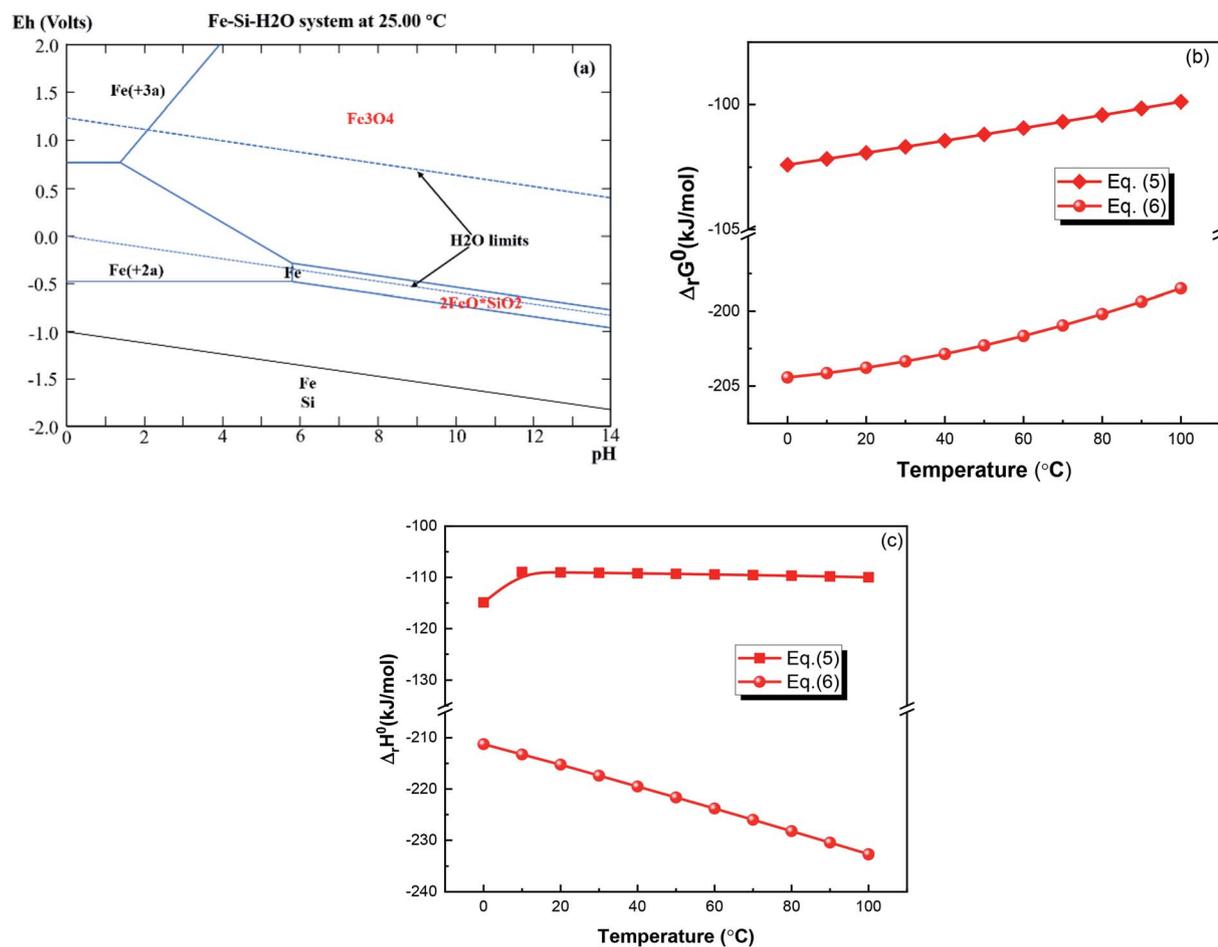

Fig. 2 (a) Eh-pH diagram of the Fe–Si–H$_2$O system at 25 °C under a_{Fe}^{2+}(aq) = 1, (b) $\Delta_r G^0$ vs. T, and (c) $\Delta_r H^0$ vs. T for eqn (5) and (6) (drawn by the HSC 6.0 chemistry software, Outokumpu Research; FactSage web, ThermFact Inc. & GTT-Technologies).
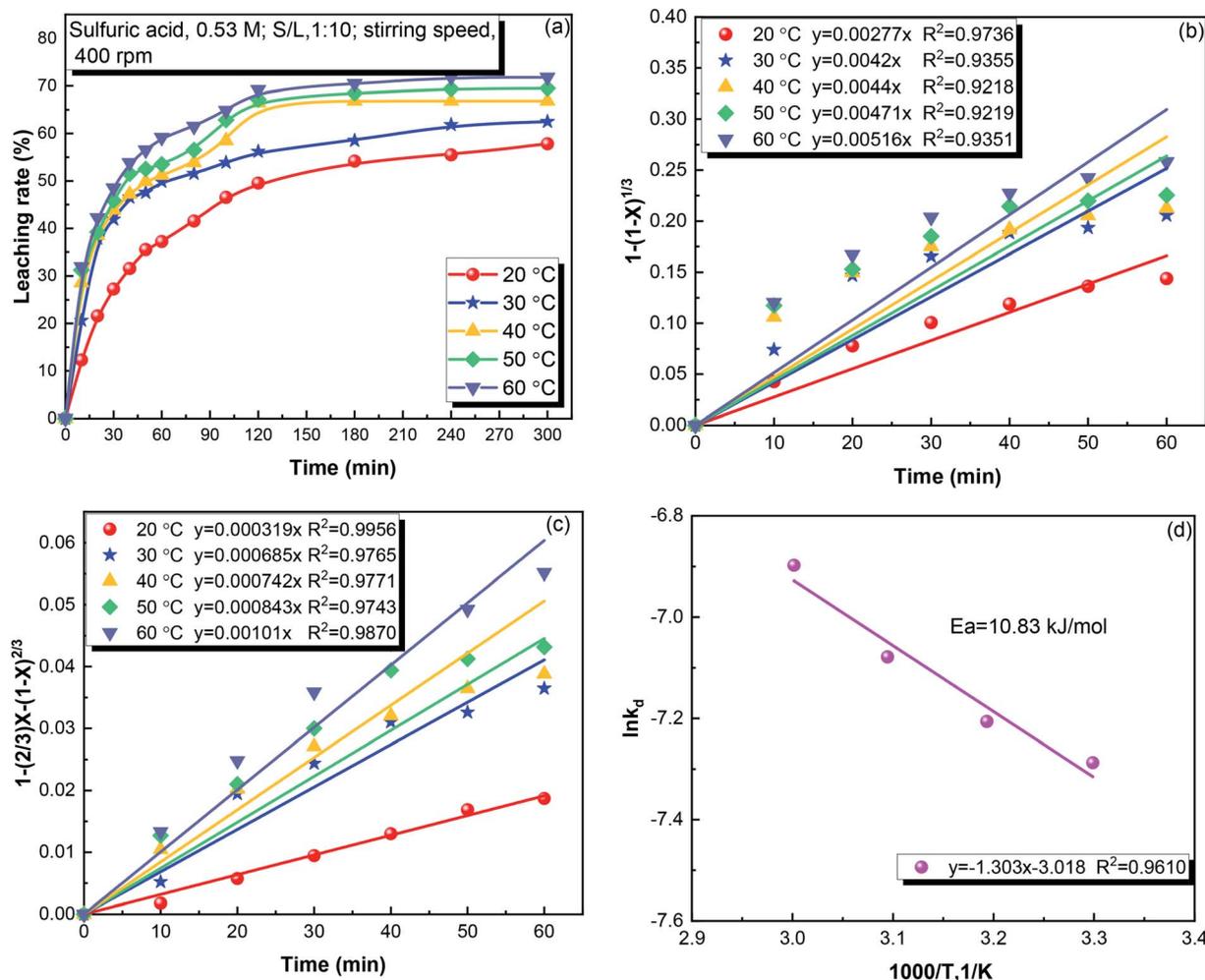
Fig. 3 (a) The effect of temperature on the leaching rate of iron from copper tailings, (b) $1 - (1 - X)^{1/3}$ versus time at different temperatures, (c) $1 - 2/3X - (1 - X)^{2/3}$ versus time at different temperatures, and (d) $\ln k_d$ versus temperature.

3. Results and discussion

3.1. Theoretical analysis of the leaching behavior of copper tailings

The leaching of copper tailings in the sulfuric acid solution may involve the reactions shown in eqn (5)–(10).[11,24,25] The Gibbs free energy ($\Delta G°$) is calculated to be -101.81 kJ mol^{-1} for Fe_3O_4, -203.58 kJ mol^{-1} for Fe_2SiO_4, -265.06 kJ mol^{-1} for CaO, -114.65 kJ mol^{-1} for CuO, -131.22 kJ mol^{-1} for ZnO, and -399.03 kJ mol^{-1} for CuS, implying that metallic oxide can be directly leached under acidic condition, while oxidation is necessary for the leaching of CuS.[26,27]

$$Fe_3O_4 + H_2SO_4 = FeSO_4 + Fe_2O_3 + H_2O \tag{5}$$

$$Fe_2SiO_4 + 2H_2SO_4 = 2FeSO_4 + H_4SiO_4 \tag{6}$$

$$CaO + H_2SO_4 = CaSO_4 + H_2O \tag{7}$$

$$CuO + H_2SO_4 = CuSO_4 + H_2O \tag{8}$$
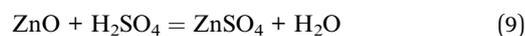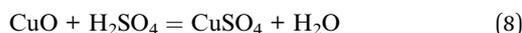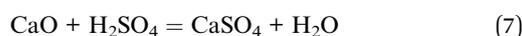
$$ZnO + H_2SO_4 = ZnSO_4 + H_2O \tag{9}$$
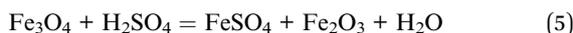
$$2CuS + O_2 + 2H_2SO_4 = 2CuSO_4 + 2S + 2H_2O \tag{10}$$

Fig. 2(a) depicts the Eh-pH diagram of the Fe–Si–H$_2$O system at 25 °C under $a_{Fe^{2+}}(aq) = 1$. Fe_3O_4 leaching requires more acidic conditions than Fe_2SiO_4, indicating that there exists a region in which Fe_2SiO_4 is leached, while Fe_3O_4 is not leached. The plots of the Gibbs free energy change versus temperature, as shown in Fig. 2(b), further indicate that Fe_3O_4 and Fe_2SiO_4 can be leached into the sulfuric acid solution. $\Delta_r H$ for both reactions is negative between 0 and 100 °C, as shown in Fig. 2(c), indicating that the two reactions are exothermic.

3.2. Leaching kinetics of iron

3.2.1. Effect of the leaching temperature.
Temperature plays a vital role in the leaching reaction.[28] The effect of temperature in the range of 20–60 °C on the leaching of iron is shown in Fig. 3. As shown in Fig. 3(a), the leaching temperature significantly affects the iron leaching. Iron leaching rapidly proceeded in the first 120 min, and then proceeded more slowly.
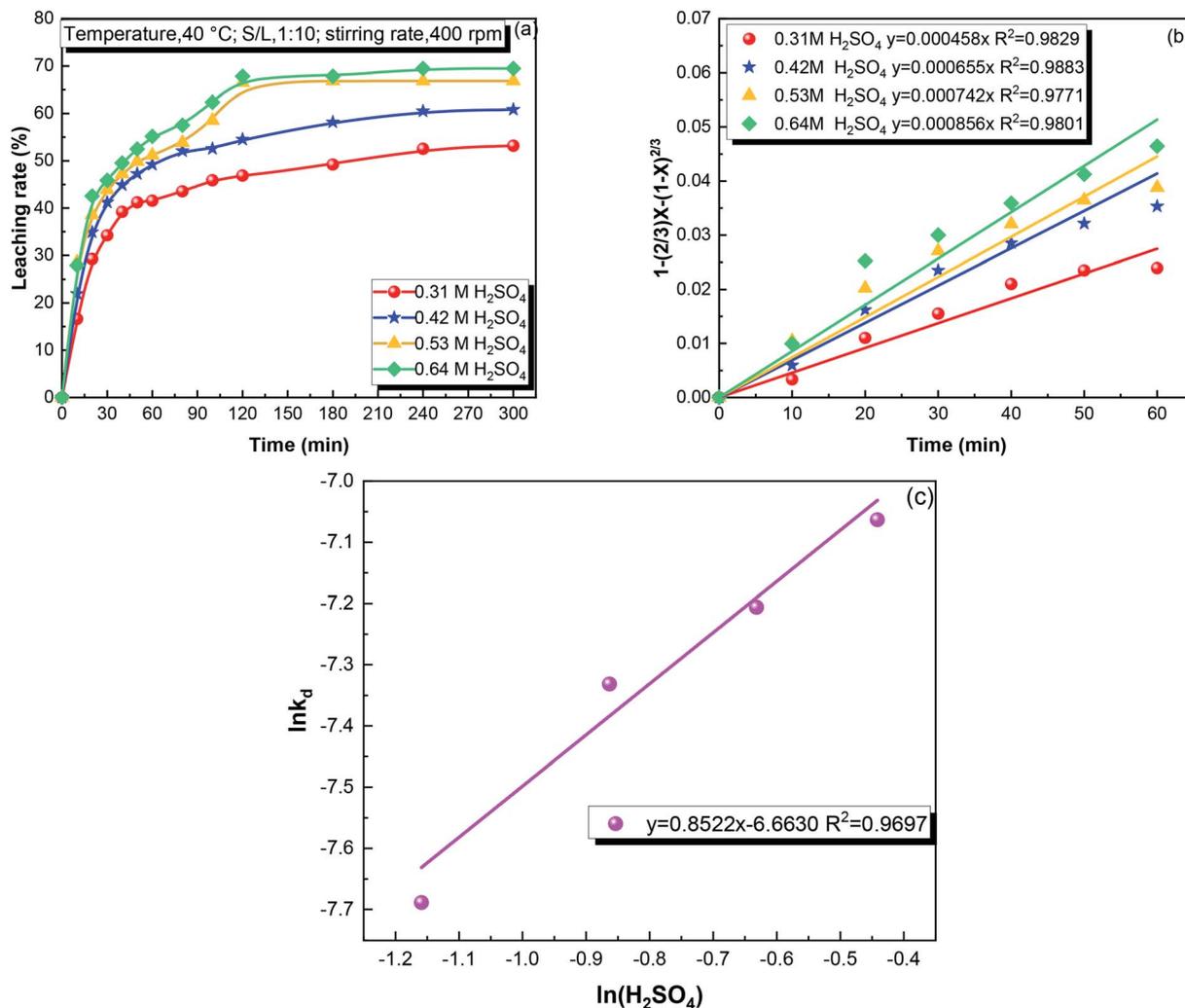
Fig. 4 (a) The effect of the sulfuric acid concentration on the leaching rate of iron from copper tailings, (b) $1 - 2/3X - (1 - X)^{2/3}$ *versus* time at different sulfuric acid concentrations, and (c) ln k_d *versus* the sulfuric acid concentration.

The leaching of iron was 49.53% at 20 °C, and increased to 69.18% at 60 °C. As shown in Fig. S1,† when the leaching temperature reached 50 °C, some of the Fe_3O_4 gradually decomposed to increase the iron ion concentration. To separate Fe_3O_4, the dissolution of Fe_3O_4 must be avoided. Thus, 40 °C was determined to be the optimum temperature, and used for subsequent experiments.

Fig. 3(b and c) shows the fits of the iron leaching results using the chemical reaction and diffusion control model, respectively. The diffusion control model provided a better fit to the data, indicating that diffusion control was the rate-limiting process. The apparent activation energy for the iron leaching from copper tailings was calculated to be 10.83 kJ mol^{-1} using the Arrhenius equation, as shown in Fig. 3(d). The apparent activation energy being below 12 kJ mol^{-1} (ref. 23) confirms that the leaching was controlled by diffusion. Moreover, the apparent activation energy was lower than that (38.69 kJ mol^{-1}) of pyrite cylinder (mainly consisting of Fe_2O_3 and Fe_3O_4),[29]

indicating that iron was not supplied by Fe_3O_4 in the copper tailings.

3.2.2. Effect of the sulfuric acid concentration. Based on eqn (6)–(9), the theoretical consumption of sulfuric acid for the leaching of CaO, CuO, and Fe_2SiO_4 from the copper tailings is about 0.53 mol L^{-1} at a S/L ratio of 1 : 10. Thus, the effect of the sulfuric acid concentration was investigated in the range of 0.31–0.64 mol L^{-1}. As shown in Fig. 4(a), the iron leaching rate increased from 46.87 to 67.83% after 120 min when the sulfuric acid concentration increased from 0.31 to 0.64 mol L^{-1}. At the sulfuric acid concentration of 0.31 mol L^{-1}, the amount of sulfuric acid was insufficient to fully leach Fe_2SiO_4. When the sulfuric acid concentration was 0.64 mol L^{-1}, some of Fe_3O_4 decomposed to increase the iron concentration in the leachate.[30]

Fig. 4(b) shows the results of these experiments fitted using the diffusion control model. The plot shown in Fig. 4(c) indicates that the reaction order with respect to the sulfuric acid concentration was 0.85.
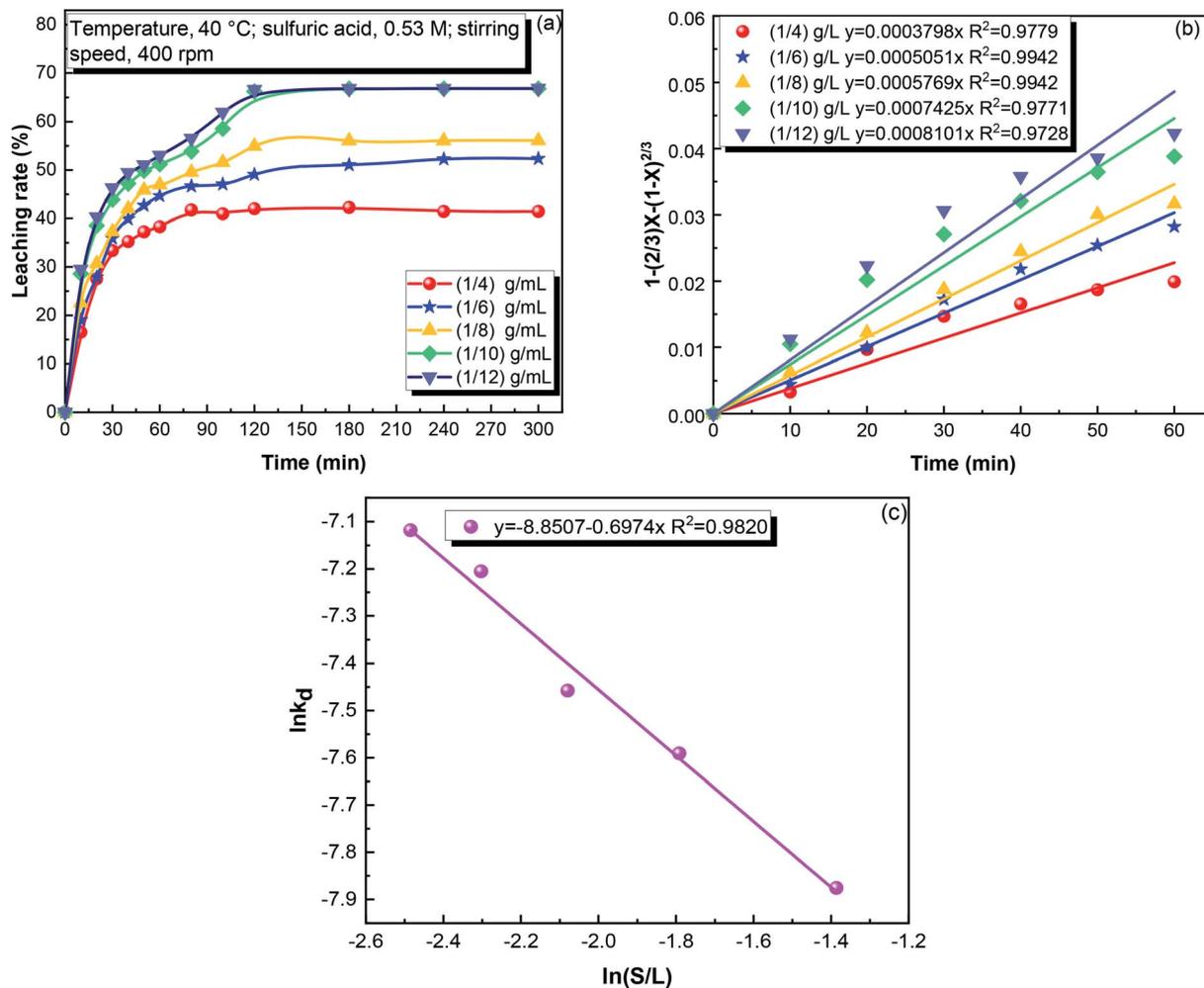
Fig. 5 (a) The effects of the S/L ratio on the leaching rate of iron from copper tailings, (b) $1 - 2/3X - (1 - X)^{2/3}$ *versus* time at different S/L ratios; and (c) ln k_d *versus* S/L ratio.

3.2.3. Effect of the S/L ratio. The effect of the S/L ratio on the iron leaching is shown in Fig. 5. As shown in Fig. 5(a), the iron leaching rate was approximately 66.50% at the S/L ratio of 1 : 12 to 1 : 10, and it decreased when the S/L ratio further increased from 1 : 10 to 1 : 4. This can be attributed to two reasons. First, a lower S/L ratio means greater possibility of the reaction of the solid with sulfuric acid. Second, a lower S/L also decreases the product diffusion resistance, favoring the iron leaching.

Fig. 5(b) shows the results of the S/L series experiments fitted using the diffusion control model, indicating that the model is consistent with this data set. Fig. 5(c) is a plot of the relationship between ln k_d and ln(S/L), showing that the reaction order with respect to the S/L ratio was −0.70.

3.2.4. Effect of the stirring speed. Stirring speed (r) affects the diffusion process during leaching. Thus, the effect of the stirring speed on the iron leaching is shown in Fig. 6. The leaching rate of iron increased significantly from 45.87 to 66.45% when the stirring speed was increased from 100 to 400 rpm, and remained unchanged with the further increase in

the stirring speed. Therefore, 400 rpm was used as the stirring speed in the other experiments.

Fig. 6(b) shows the fitting results of the stirring speed experiments using the diffusion control model. The model is consistent with this data set. Fig. 6(c) plots the relationship between ln k_d and ln r, showing that the reaction order with respect to the stirring speed was 0.40 for the iron leaching.

3.2.5. Kinetic model. According to the experimental results described above, the leaching of iron from copper tailings was determined to be controlled by the product diffusion model. The leaching of iron can be expressed by the following equation.

$$1 - \frac{2}{3}X - (1 - X)^{\frac{2}{3}} = K_d t$$

$$= k_0 [H_2SO_4]^{0.85} \left(\frac{S}{L}\right)^{-0.70} r^{0.40} \exp\left(-\frac{10.83}{RT}\right) t \quad (11)$$

where X is the fraction of iron reacted, k_0 is the correlation coefficient, $[H_2SO_4]$ is the concentration of sulfuric acid (mol L^{-1}), S/L is the ratio of solid to liquid, and r is the stirring speed (rpm).
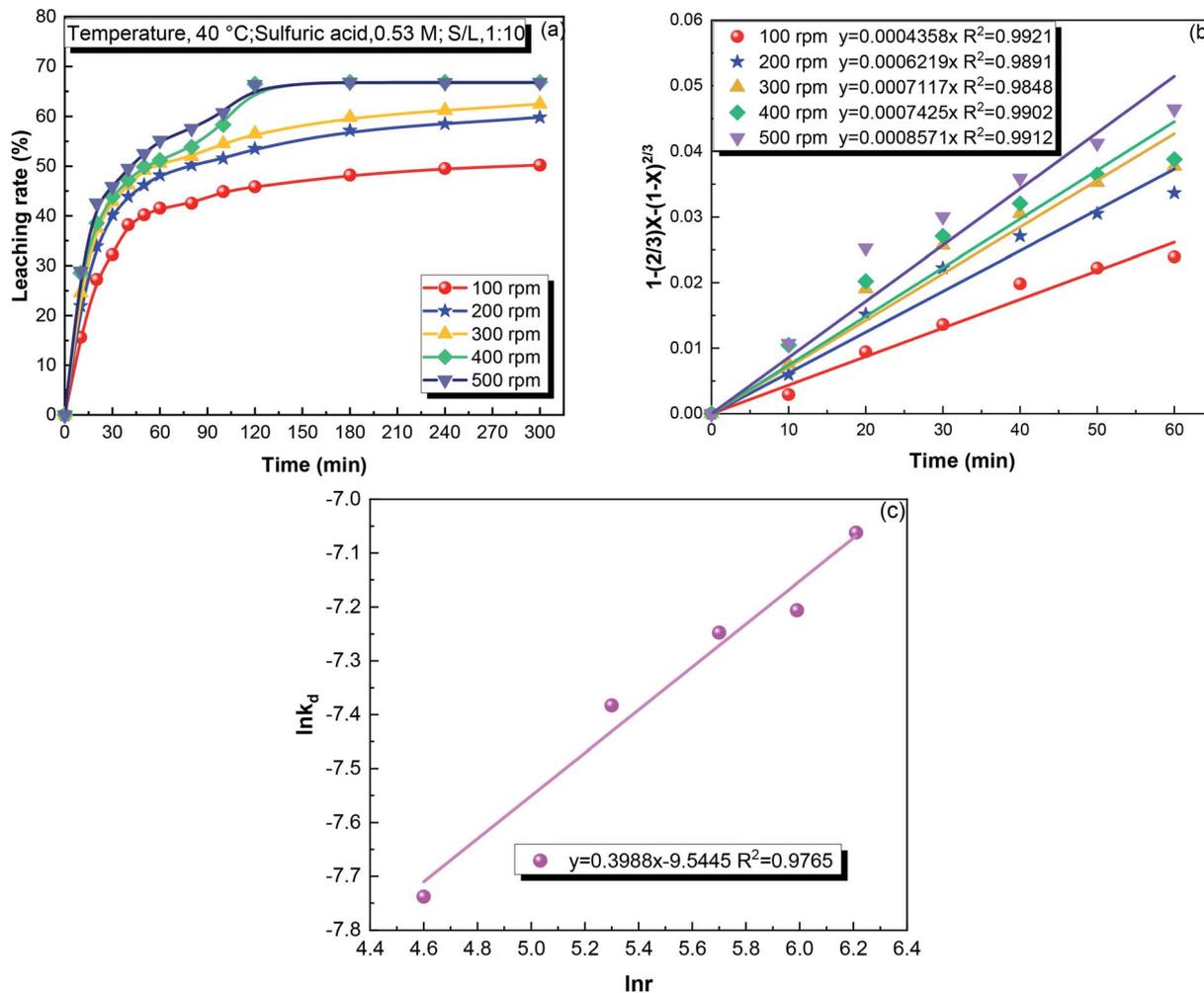
Fig. 6 (a) The effect of the stirring speed on the leaching rate of iron from copper tailings, (b) $1 - 2/3X - (1-X)^{2/3}$ *versus* time at different stirring speeds, and (c) ln k_d *versus* the stirring speed.

3.3. Leaching behaviors of Ca, Zn, Cu and Si

As the other main elements in the copper tailings, the leaching behaviors of Ca, Zn, Cu, and Si were studied, as presented in Fig. 7. The sulfuric acid concentration significantly affected the leaching rate of Zn and Si, while it had no effect on the leaching of Ca and Cu. When the sulfuric acid concentration was
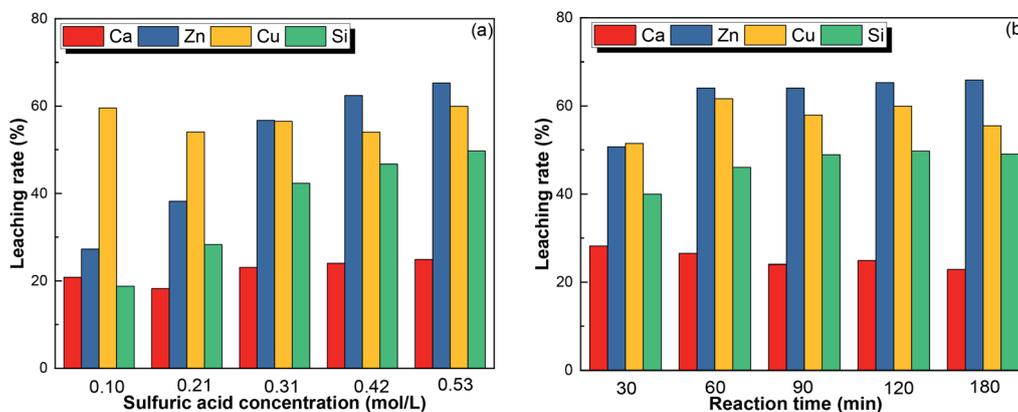

Fig. 7 The leaching rate of Cu, Zn, Ca, and Si at (a) different sulfuric acid concentrations, and (b) different leaching times under the optimum conditions.
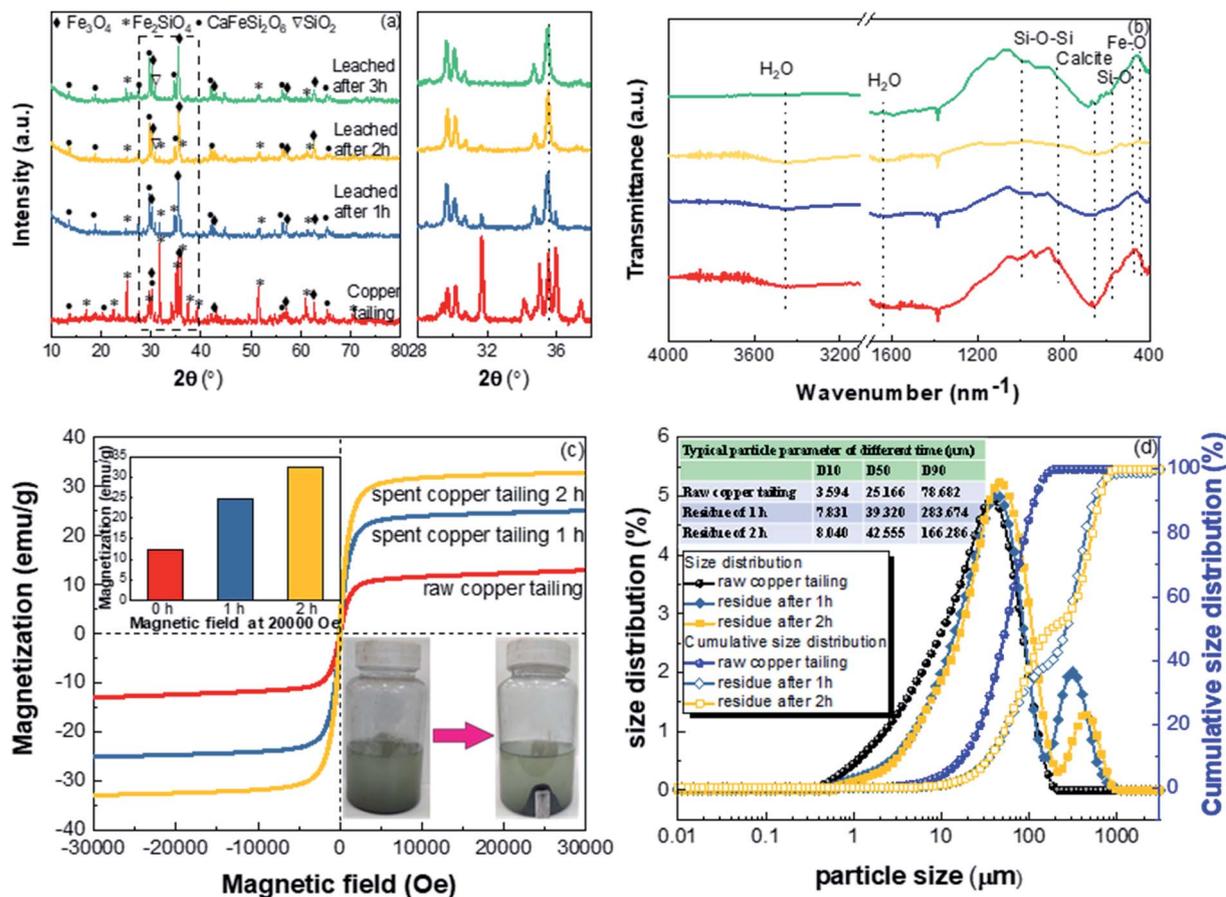
Fig. 8 (a) XRD patterns, (b) FTIR spectra, (c) magnetic hysteresis loops, and (d) PSD of raw and leached copper tailings.

increased from 0.10 to 0.53 mol L^{-1}, the leaching rate increased from 27.23 to 65.32% for Zn and from 18.80 to 49.03% for Si. The leaching rate was constant at roughly 20% for Ca and 59% for Cu, respectively, indirectly indicating that Ca and Cu were more easily leached from the copper tailings. As shown in Fig. 7(b), at S/L of 1 : 10 and sulfuric acid concentration of 0.53 mol L^{-1}, Ca was the first element to achieve an optimal leaching rate, followed by Zn and Cu. The leaching rate of Zn increased from 50.70 to 64.08% when the leaching time increased from 30 to 60 min. These results are consistent with the mineral composition of copper tailings.[31–34] Regarding the recovery of metals, Fig. S3† demonstrates a process route for the recovery of metals based on fractional precipitation,[35] providing a possible way to recover Cu, Zn, and Fe.

3.4. Characterization of the raw and treated copper tailings

3.4.1. XRF. The concentrations (by weight) of the major elements in the raw and leached copper tailings are listed in Table 1. After 2 h of leaching, the Fe content decreased from 36.76% to 28.44%, Zn decreased from 2.06% to 1.69%, and Cu decreased from 0.26% to 0.24%. It shows that Fe, Zn, and Cu were leached differently in the process, which may be attributed to the crystal structure and morphology of copper tailings. Theoretically, the Fe contents in pure Fe_2SiO_4, Fe_3O_4, and

$CaFeSi_2O_6$ are 54.81%, 72.35%, and 22.51%, while the Si contents in pure Fe_2SiO_4 and $CaFeSi_2O_6$ are 13.78% and 22.64%, respectively. The presence of Ca, Fe, and Si in the leached copper tailings indicates that it can be used as cement raw materials, avoiding secondary pollution.[36]

3.4.2. XRD, FTIR, magnetization, and particle size. Fig. 8(a) shows the XRD patterns of raw and leached copper tailings. Fe_2SiO_4, Fe_3O_4, and $CaFeSi_2O_6$ are the main crystalline phases of the raw copper tailings. During the leaching process, most of Fe_2SiO_4 gradually disappeared, while peak intensity related to Fe_3O_4 and $CaFeSi_2O_6$ were relatively stable. The results are consistent with the thermodynamic calculations and mineral properties.[37]

FT-IR spectra of the raw and leached copper tailings are shown in Fig. 8(b). The absorption peaks at around 1640 cm^{-1} are ascribed to O–H bending vibrations, peaks at around 1097 cm^{-1} correspond to the symmetrical stretching vibrations of Si–O–Si, and peaks at about 798 and 467 cm^{-1} correspond to the symmetrical stretching vibrations of Si–O.[38,39] After leaching, the intensity of the Si–O stretching vibration peak slightly weakened, while the other main peaks remained almost identical. This is consistent with the dissolution of Fe_2SiO_4, while the other main structures of the copper tailings were stable during the leaching.
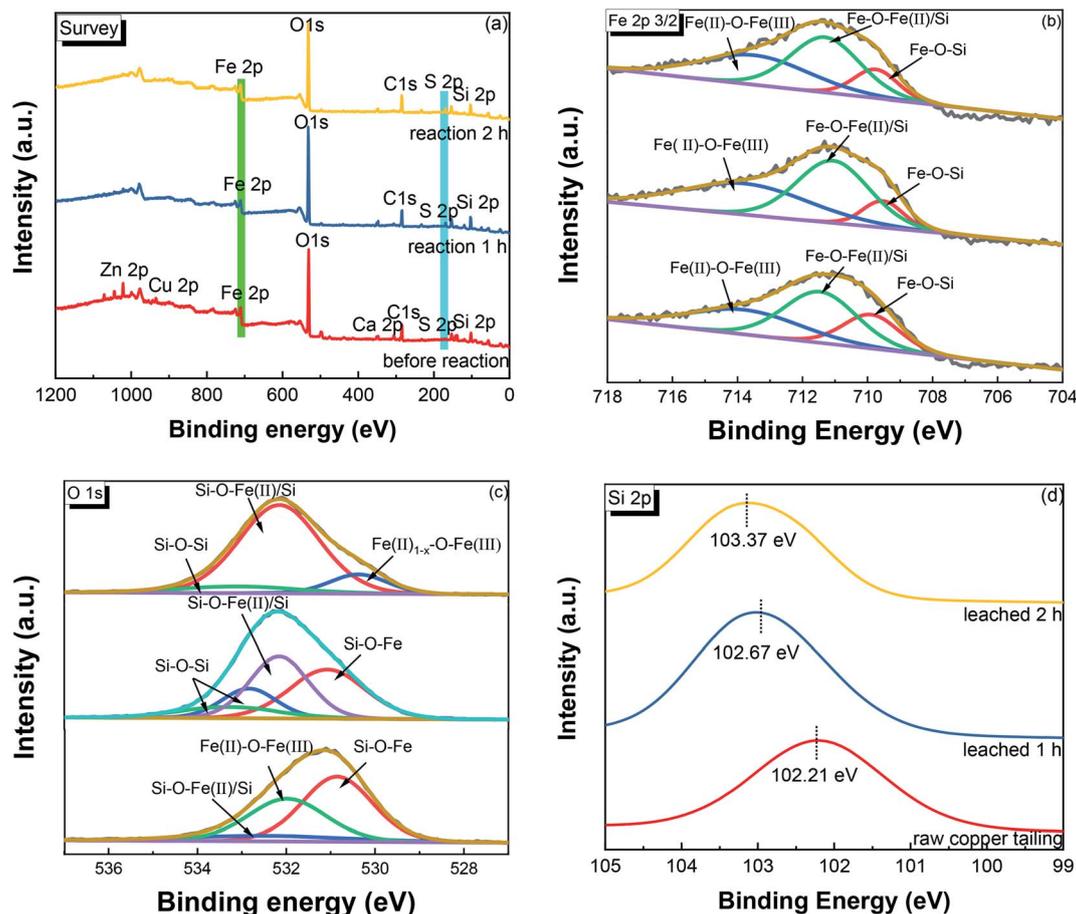
Fig. 9 XPS spectra of the raw and leached copper tailings. (a) Survey scan, and detailed scans in the (b) Fe 2p, (c) O 2p, and (d) Si 2p regions.

To further verify the identity of the species involved in acid leaching, the magnetic properties of ferrite were investigated at room temperature using PPMS DynaCool, and the results are shown in Fig. 8(c). The magnetic properties of the copper tailings increased with leaching. The reason for this is that the nonmagnetic components and the weakly magnetic Fe(II) in fayalite were leached by the acid and migrated to the liquid.

The particle size distributions of raw and leached copper tailings are plotted in Fig. 8(d). The average particle sizes of the raw copper tailings and residuals after 1 h and 2 h of leaching were 25.2, 39.3, and 42.6 μm, respectively. Compared to the raw copper tailings, the average particle size of the leached copper tailings did not change noticeably, further indicating that the leaching process followed the shrinking core model. Moreover, particles in the size range of 211.0–974.5 μm were found in the leached copper tailings, which are due to the formation of insoluble substances, including $CaSO_4$ and SiO_2.

3.4.3. XPS. To further investigate the chemical changes involved in the leaching process, XPS data were collected for the

Table 2 Peak positions, full width at half maximum (FWHM), and relative abundance of chemical states from fitting the Fe $2p_{2/3}$ feature from raw and leached copper tailings

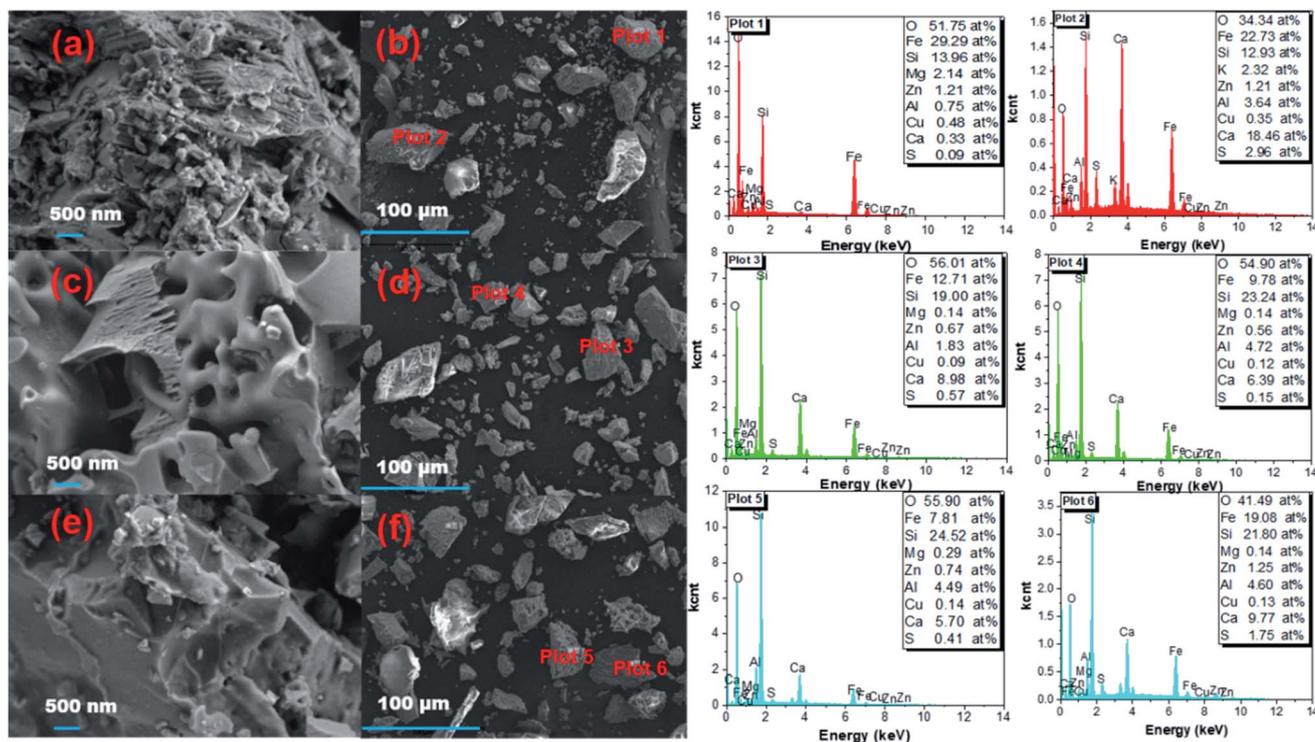| Sample	BE (eV)	FWHM (eV)	State of iron	Percentage (%)
Raw copper tailings	709.88	2.04	Si–O–Fe(II)	22.59
	713.79	4.11	Fe(II)–O–Fe(III)	33.08
	711.46	2.66	Fe–O–Fe(II)/Si	44.33
Copper tailings after leaching 1 h	709.50	1.45	Si–O–Fe(II)	11.24
	713.75	4.64	Fe(II)–O–Fe(III)	41.61
	711.04	2.62	Fe–O–Fe(II)/Si	47.14
Copper tailings after leaching 2 h	709.72	1.60	Si–O–Fe(II)	15.16
	713.45	3.95	Fe(II)–O–Fe(III)	38.72
	711.28	2.52	Fe–O–Fe(II)/Si	46.11

Fig. 10 SEM/EDS analysis of raw and leached copper tailings. (a and b) Raw copper tailings, (c and d) copper tailings after leaching for 1 h, and (e and f) copper tailings after leaching for 2 h.

Fe 2p, O 1s, and Si 2p core levels from raw and leached copper tailings.

The survey scans in Fig. 9(a) show that the relative intensity of the Fe 2p and Zn 2p peaks decreased, while a relatively stronger S 2p characteristic peak could be observed from the samples after acid leaching, which is consistent with the XRF result and which might be due to the deposition of sulfate in the leached copper tailings. Fig. 9(b) shows the XPS spectra of Fe 2p, where the binding energy of 713.79 eV is attributed to $Fe(II)–O–Fe(III)$, while the peak at 709.88 eV corresponds to Si–O–Fe.[40] A summary of the Fe 2p fitting results and the Fe chemical state in the near surface region is shown in Table 2. The relative content of Si/Fe–O–Fe decreased from 66.92% to 61.27%, while that of

$Fe(II)–O–Fe(III)$ increased from 33.08% to 38.73% during leaching, implying that Fe^{2+} was leached from Fe_2SiO_4. Fig. 9(c) shows the O 1s spectra, which indicated that Si–O–Si was present in the leached copper tailings.[41] The binding energy of O 1s shifted to a higher energy after leaching. The relative abundance result (Table S1†) indicated that SiO_2 was generated in the process. The Si 2p feature also shifted to a higher binding energy after leaching, as shown in Fig. 9(d), indicating the decrease in the electron density near the silicon atoms.[40,41]

3.4.4. SEM/EDS. Images showing the morphology of the raw and leached copper tailings are presented in Fig. 10. The raw copper tailing appeared as compact and uneven solid (Fig. 10(a and b)). In comparison, some irregular holes and
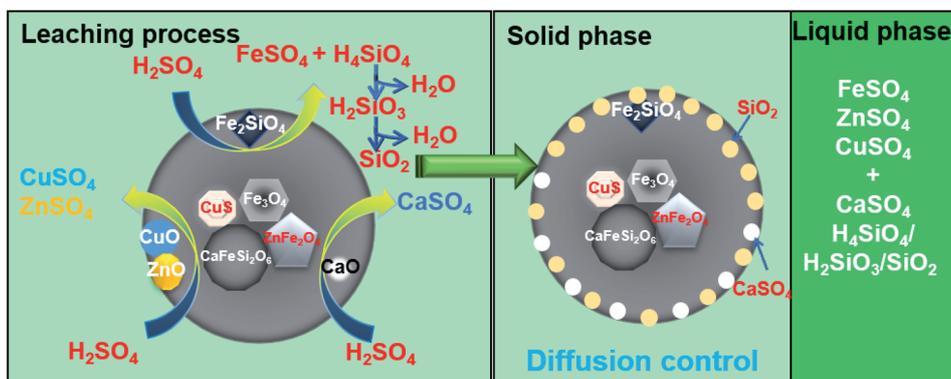

Fig. 11 Schematic of the mechanism of the sulfuric acid leaching of copper tailing.

small loose particles were observed in the leached copper tailings (Fig. 10(c–f)). The related EDS analysis indicated that during leaching Fe was extracted, while the content of S and Si increased. Small particles ($CaSO_4$ and SiO_2) may accumulate and cover the surface of copper tailing, thus impeding the sulfuric acid from diffusing to the interior of the particles and leaching the iron.

3.5. Mechanism of leaching

Based on the results discussed above, a leaching mechanism can be proposed, which is shown in Fig. 11. When the copper tailings are contacted with sulfuric acid, oxides (including CaO, CuO, and ZnO) from the copper tailings preferentially react with sulfuric acid, generating sulfates (including $CaSO_4$, $CuSO_4$, and $ZnSO_4$).[11,24,25] Subsequently, Fe_2SiO_4 reacts with sulfuric acid, thus generating $FeSO_4$ and H_4SiO_4. As the reaction proceeds, H_4SiO_4 is partly converted into H_2SiO_3 and SiO_2.[42] The accumulation of SiO_2 and $CaSO_4$ reduces the contact of sulfuric acid with the soluble iron of copper tailings, thus inhibiting the further leaching of iron. Sulfuric acid concentration and temperature both have a significant effect on leaching process. When the sulfuric acid concentration reached 0.53 mol L^{-1}, FeO from Fe_3O_4 was slightly decomposed.[25] However, an excess of sulfuric acid would destroy the leaching system due to the rapid formation of H_4SiO_4 by the quick dissolution of Fe_2SiO_4.[11] The elevated temperature enhances the leaching of metal ions and oxidation of Fe^{2+} to Fe^{3+}. In the presence of Fe^{3+}, the copper leaching rate is enhanced.[43]

4. Conclusions

In this study, the leaching characteristics of the major metal components from copper tailings by sulfuric acid were investigated, with a particular focus on iron. After 120 min, 66.45% of Fe, along with 65.32% of Cu and 59.95% of Zn in the tailings were leached under the optimal conditions of 40 °C, sulfuric acid concentration of 0.53 mol L^{-1}, stirring speed of 400 rpm, and solid/liquid ratio of 1 : 10. The iron leaching was found to be controlled by the product diffusion model with an apparent activation energy of 10.83 kJ mol^{-1}. The reaction orders for the sulfuric acid concentration, stirring speed, and solid/liquid ratio were 0.85, −0.70, and 0.40, respectively. During leaching, the amount of Fe_2SiO_4 in copper tailings was obviously reduced, while that of Fe_3O_4 remained stable. The accumulation of $CaSO_4$ and SiO_2 inhibited the further leaching of iron.

Conflicts of interest

There are no conflicts to declare.

Acknowledgements

References

1 Z. L. Zuo, Q. B. Yu, S. Y. Luo, J. K. Zhang and E. Z. Zhou, *Energy Fuels*, 2020, **34**, 491–500.

2 R. Sharma and R. A. Khan, *J. Clean Prod.*, 2018, **171**, 1171–1186.

3 F. Vargas and M. Lopez, *J. Clean Prod.*, 2018, **182**, 427–436.

4 B. Mikoda, H. Kucha, A. Potysz and E. Kmiecik, *Appl. Geochem.*, 2018, **98**, 459–472.

5 Z. Q. Guo, J. Pan, D. Q. Zhu and F. Zhang, *J. Clean Prod.*, 2018, **199**, 891–899.

6 A. Jarosikova, V. Ettler, M. Mihaljevic, B. Kribek and B. Mapani, *J. Environ. Manage.*, 2017, **187**, 178–186.

7 S. W. Zhou, Y. G. Wei, B. Li and H. Wang, *J. Clean Prod.*, 2019, **217**, 423–431.

8 S. W. Zhou, Y. G. Wei, S. Y. Zhang, B. Li, H. Wang, Y. D. Yang and M. Barati, *J. Clean Prod.*, 2019, **236**, 117668.

9 I. Fuentes, C. Ulloa, R. Jiménez and X. García, *J. Hazard. Mater.*, 2020, **387**, 121693.

10 M. K. Khalid, J. Hamuyuni, V. Agarwal, J. Pihlasalo, M. Haapalainen and M. Lundström, *J. Clean Prod.*, 2019, **215**, 1005–1013.

11 M. I. Muravyov, N. V. Fomchenko, A. V. Usoltsev, E. A. Vasilyev and T. F. Kondrat'eva, *Hydrometallurgy*, 2012, **119–120**, 40–46.

12 S. Stankovic, I. Moric, A. Pavic, S. Vojnovic, B. Vasiljevic and V. Cvetkovic, *J. Serb. Chem. Soc.*, 2015, **80**, 391–405.

13 B. Han, B. Altansukh, K. Haga, Z. Stevanovic, R. Jonovic, L. Avramovic, D. Urosevic, Y. Takasaki, N. Masuda, D. Ishiyama and A. Shibayama, *J. Hazard. Mater.*, 2018, **352**, 192–203.

14 G. C. Shi, Y. L. Liao, B. W. Su, Y. Zhang, W. Wang and J. J. Xi, *Sep. Purif. Technol.*, 2020, **241**, 116699.

15 L. Tao, X. Q. Wang, P. Ning, L. L. Wang and W. J. Fan, *Fuel Process. Technol.*, 2019, **192**, 36–44.

16 H. Wang, B. Yuan, R. L. Hao, Y. Zhao and X. P. Wang, *Chem. Eng. J.*, 2019, **378**, 122155.

17 X. S. Meng, S. A. Khoso, J. H. Kang, J. Q. Wu, J. D. Gao, S. Y. Lin, M. R. Wu, W. Sun and Y. H. Hu, *J. Clean Prod.*, 2019, **241**, 118371.

18 Z. D. Yuan, G. Q. Zhang, X. Ma, L. Yu, X. Wang, S. F. Wang and Y. F. Jia, *Chem. Eng. J.*, 2019, **378**, 122126.

19 Y. K. Li, X. Zhu, X. J. Qi, B. Shu, X. Zhang, K. Z. Li, Y. G. Wei and H. Wang, *Chem. Eng. J.*, 2020, **394**, 124833.

20 J. Mu, Z. Y. Hu, L. J. Huang, Z. J. Xie and P. E. Holm, *Environ. Pollut.*, 2020, **257**, 113565.

21 M. Rogowski, T. Smolinski, M. Pyszynska, M. Brykala and A. G. Chmielewski, *Nukleonika*, 2018, **63**, 131–137.

22 C. Zhang, X. B. Min, J. Q. Zhang, M. Wang, Y. C. Li and J. C Fei, *J. Clean Prod.*, 2016, **113**, 910–918.

23 M. Li, S. L. Zheng, B. Liu, H. Du, D. B. Dreisinger, L. Tafaghodi and Y. Zhang, *Waste Manag.*, 2017, **65**, 128–138.

24 E. H. Oelkers, J. Declercq, G. D. Saldi, S. R. Gislason and J. Schott, *Chem. Geol.*, 2018, **500**, 1–19.

25 A. H. Kaksonen, S. Särkijärvi, E. Peuraniemi, S. Junnikkala, J. A. Puhakka and O. H. Tuovinen, *Hydrometallurgy*, 2017, **168**, 135–140.

26 A. Muszer, J. Wodka, T. Chmielewski and S. Matuska, *Hydrometallurgy*, 2013, **137**, 1–7.

27 J. Lee, S. Kim, B. Kim and J. C. Lee, *Metals*, 2018, **8**, 9.

28 J. Y. Ma, Y. F. Zhang, Y. H. Qin, Z. K. Wu, T. L. Wang and C. W Wang, *Ultrason. Sonochem.*, 2017, **35**, 304–312.

29 Z. Z. Shi, M. R. Wang, G. K. Zhang and L. Zhang, *Asian J. Chem.*, 2013, **25**, 105–109.

30 L. Deng, B. Qu, S. Su, S. Ding and W. Sun, *Arabian J. Sci. Eng.*, 2018, **44**, 5335–5344.

31 Y. J. Wang, S. M. Wen, Q. C. Feng, Y. J. Xian and D. Liu, *Russ. J. Non-Ferrous Met.*, 2015, **56**, 127–133.

32 Y. Li, H. Liu, B. Peng, X. Min, M. Hu, N. Peng, Y. Yuang and J. Lei, *Hydrometallurgy*, 2015, **158**, 42–48.

33 D. M. Urosevic, M. D. Dimitrijevic, Z. D. Jankovic and D. V. Antic, *Physicochem. Probl. Miner. Process*, 2015, **51**, 73–82.

34 A. Krol, K. Mizerna and M. Bozym, *J. Hazard. Mater.*, 2019, 121502, DOI: 10.1016/j.jhazmat.2019.121502.

35 L. Fang, L. Li, Z. Qu, H. M. Xu, J. F. Xu and N. Q. Yan, *J. Hazard. Mater.*, 2018, **342**, 617–624.

36 L. Tang, C. B. Tang, J. Xiao, P. Zeng and M. T. Tang, *J. Clean Prod.*, 2018, **201**, 764–773.

37 F. Ruan, S. Kawanishi, S. Sukenaga and H. Shibata, *ISIJ Int.*, 2020, **60**, 419–425.

38 Y. X. Nie, S. Li, C. Wu, C. Wang, D. D He and Y. Mei, *Ind. Eng. Chem. Res.*, 2018, **57**, 15138–15146.

39 M. Ye, G. Li, P. Yan, J. Ren, L. Zheng, D. Han, S. Sun, S. Huang and Y. Zhong, *Chemosphere*, 2017, **185**, 1189–1196.

40 Z. B. Wang, Z. W. Zhao, L. F. Zhang, F. S. Liu, B. Peng, L. Y. Chai, D. C. Liu, D. G. Liu, T. Y. Wang, H. Liu and Y. J. Liang, *J. Hazard. Mater.*, 2019, **364**, 488–498.

41 Z. B. Wang, B. Peng, L. F. Zhang, Z. W. Zhao, D. G. Liu, N. Peng, D. W. Wang, Y. H. He, Y. J. Liang and H. Liu, *JOM*, 2017, **70**, 539–546.

42 F. Carranza, N. Iglesias, A. Mazuelos, R. Romero and O. Forcat, *Miner. Eng.*, 2009, **22**, 107–110.

43 M. M. Antonijevic, M. D. Dimitrijevic, Z. O. Stevanovic, S. M. Serbula and G. D. Bogdanovic, *J. Hazard. Mater.*, 2008, **158**, 23–34.